Published in final edited form as:
J Biol Chem. 2002 May 24; 277(21): 18868–18874. doi:10.1074/jbc.M201463200.

Biochemical and Structural Definition of the l-Afadin- and Actin-binding Sites of α-Catenin*

Sabine Pokutta[‡,§], **Frauke Drees**[§], **Yoshimi Takai**[¶], **W. James Nelson**[§], and **William I. Weis**[‡,§,‖]

[‡]Department of Structural Biology, Stanford University School of Medicine, Stanford, California 94305

[§]Department of Molecular and Cellular Physiology, Stanford University School of Medicine, Stanford, California 94305

[¶]Department of Molecular Biology and Biochemistry, Osaka University Graduate School of Medicine, Suita 565-0871, Japan

Abstract

α -Catenin is an integral component of adherens junctions, where it links cadherins to the actin cytoskeleton. α-Catenin is also required for the colocalization of the nectin/afadin/ponsin adhesion system to adherens junctions, and it specifically associates with the nectin-binding protein afadin. A proteolytic fragment of α-catenin, residues 385–651, contains the afadin-binding site. The three-dimensional structure of this fragment comprises two side-by-side four-helix bundles, both of which are required for afadin binding. The α-catenin fragment 385–651 binds afadin more strongly than the full-length protein, suggesting that the full-length protein harbors a cryptic binding site for afadin. Comparison of the α-catenin 385–651 structure with the recently solved structure of the α-catenin M-fragment (Yang, J., Dokurno, P., Tonks, N. K., and Barford, D. (2001) *EMBO J.* 20, 3645–3656) reveals a surprising flexibility in the orientation of the two four-helix bundles. α-Catenin and the actin-binding protein vinculin share sequence and most likely structural similarity within their actin-binding domains. Despite this homology, actin binding requires additional sequences adjacent to this region.

Specific cell-cell contacts establish and maintain the complex architecture of tissues (1). These contacts are highly dynamic and regulated during morphogenesis or tissue remodeling, and must be strong enough to withstand mechanical stresses placed upon the tissue. In polarized epithelial cells, three different types of cell-cell junctions, tight junctions, adherens junctions, and desmosomes, are aligned along the apical-basal axis of the lateral membrane.

*This work was supported by Grants GM35227 (to W. J. N.) and GM56169 (to W. I. W.) from the National Institutes of Health. Portions of this work were carried out at the Stanford Synchrotron Radiation Laboratory (SSRL), a national user facility operated by Stanford University on behalf of the United States Department of Energy, Office of Basic Energy Sciences. The SSRL Structural Molecular Biology Program is supported by the Department of Energy, Office of Biological and Environmental Research, and by the National Institutes of Health, National Center for Research Resources, Biomedical Technology Program, and the National Institute of General Medical Sciences.

‖To whom correspondence should be addressed: Dept. of Structural Biology, Stanford University School of Medicine, Fairchild Bldg., 299 Campus Dr. West, Stanford, CA 94305. Tel.: 650-725-4623; Fax: 650-723-8464; bill.weis@stanford.edu.

The atomic coordinates and structure factors (code 1L7C) have been deposited in the Protein Data Bank, Research Collaboratory for Structural Bioinformatics, Rutgers University, New Brunswick, NJ (http://www.rcsb.org/).

In adherens junctions, classical cadherins function as homophilic adhesion molecules. Clustering of cadherins and their attachment to the actin cytoskeleton are key steps in the assembly of functional adherens junctions. Cadherin clustering facilitates formation of lateral cis-dimers between cadherin molecules on the same cell surface. Cis-dimers have a much higher activity for adhesive trans-interaction between molecules on opposing cells (2–4). Anchorage to the cytoskeleton may promote cis-dimerization and higher order clustering and thereby contribute to strengthening of cell adhesion (5, 6).

Linkage of classical cadherins to the cytoskeleton is mediated by proteins termed catenins. β-Catenin and plakoglobin (γ-catenin) both bind in a mutually exclusive manner to the cytoplasmic domain of classical cadherins, and interact with α-catenin (7, 8). α-Catenin links the cadherin-β-catenin/plakoglobin complex to the cytoskeleton either through direct binding to F-actin (9) or indirectly through the interaction with the actin-binding proteins vinculin, α-actinin, ZO-1, or ZO-2 (10–14). Additionally, α-catenin interacts with spectrin, which might play a role in assembly of the cortical spectrin cytoskeleton (15). The diversity of these binding partners indicates that α-catenin plays a key role in assembly of adherens junctions.

In adherens junctions of polarized epithelial cells, the nectin/ afadin/ponsin (NAP)[1] cell adhesion system colocalizes with cadherins (16, 17). Nectin is a homophilic cell adhesion protein of the immunoglobulin superfamily. Afadin, an F-actin-binding protein, contains a PDZ domain that binds to the cytoplasmic domain of nectin (16, 18). Afadin exists in two splice variants: l-afadin is expressed ubiquitously, whereas s-afadin is found only in neural tissues (18). Like cadherins, nectin forms cis-dimers, which might be required for trans-interactions (19). Binding of afadin to the cytoplasmic domain of nectin is not required for cis- or trans-interactions, but it is required for clustering of nectin molecules in cell-cell contact sites and for colocalization of the NAP adhesion system with cadherins (19). Analysis of afadin (−/−) mice shows that afadin is essential for proper organization of adherens junctions and tight junctions in epithelial cells (20).

The colocalization of the NAP adhesion system with adherens junctions depends upon afadin and α-catenin (21). However, initial attempts to demonstrate a direct interaction between afadin and α-catenin using recombinant full-length proteins failed (22). Recently a direct interaction between the C-terminal half of α-catenin and afadin was shown by yeast two hybrid and *in vitro* binding analysis (21). The observation that a truncated form, but not full-length α-catenin, binds to afadin suggests that afadin binding is regulated through exposure of a cryptic binding site in α-catenin.

We present here the structure of a proteolytically derived fragment of α-catenin, residues 385–651, and demonstrate that it comprises the l-afadin-binding site. Structural and biochemical data suggest mechanisms for unmasking the cryptic l-afadin-binding site in α-catenin. α-Catenin is homologous to the actin-binding protein vinculin. Structural similarity has been proposed for the two proteins for more than 80% of their sequence (23–27). Despite strong sequence homology between the actin-binding region of vinculin and a C-terminal portion of α-catenin, we show that α-catenin requires additional sequences for binding to actin.

[1]The abbreviations used are: NAP, nectin/afadin/ponsin; GST, glutathione *S*-transferase; DTT, dithiothreitol; MDCK, Madin-Darby canine kidney; ERM, ezrin/radixin/moesin; DMS, dimethyl suberimidate.

EXPERIMENTAL PROCEDURES

Construction of Expression Vectors

Full-length α-catenin used in the limited proteolysis experiment was expressed with a C-terminal His_6-tag (28); for expression of the N-terminal GST fusion protein, full-length α-catenin was inserted into the pGEX-KG vector, a modified form of pGEX-2T (Amersham Biosciences), in which a linker of 5 glycine residues is introduced between the thrombin cleavage and the multiple cloning sites (29).[2] All α-catenin fragments were amplified by PCR. α-Catenin 385–651 and α-catenin 385–507 were cloned into the pGEX-2T expression vector (Amersham Biosciences). α-Catenin 632–906, α-catenin 671–906, and α-catenin 678 – 864 were cloned into the pGEX-4T-3 vector (Amersham Biosciences), and α-catenin 507–632 was introduced into the pGEX-KG vector.

Protein Expression and Purification

GST-full-length α-catenin was expressed in *E. coli* Ab1899 cells, and all other GST fusion proteins were expressed in *E. coli* BL21 cells. Bacteria were grown at 37 °C in LB in the presence of 100 μg/ml ampicillin until an A_{600} of 0.8–1.0 was reached. Cells were induced with 1 mM isopropyl-g-D-thiogalactopyr-anoside and grown for an additional 4 h. After centrifugation, the pelleted cells were resuspended in 50 mM Tris, pH 8.0, containing 2 mM EDTA, 0.1% Triton X-100, 1 mM DTT, 2.5 mM phenylmethylsulfonyl fluoride, 2.5 μg/ml aprotinin, 5 μg/ml pepstatin, and lysed by passage through a French pressure cell. The lysate was cleared by centrifugation and subsequently incubated with glutathione-agarose for 1 h at 4 °C. α-Catenin 385–651, α-catenin 385–507, and α-catenin 507–632 were cleaved from the GST-tag with trypsin (L-1-tosylamido-2-phenyl-ethyl chloromethyl ketone (TPCK)-treated, Sigma) (4.8, 48, and 240 units/ml of 50% beads, respectively, for 1 h at room temperature), whereas α-catenin 632–906, α-catenin 671–906, and α-catenin 678 – 864 were cleaved with bovine thrombin (Sigma) (1.1, 6.6, and 7.6 units/ml of 50% beads for 1 h at room temperature). GST fusion proteins were eluted from the beads with 20 mM Tris, pH 8.5, 150 mM NaCl, 1 mM DTT, 50 mM reduced glutathione. The proteins were further purified by anion exchange chromatography (Mono Q column, Amersham Biosciences) or in case of α-catenin 678 – 864 and α-catenin 671–906 by cation exchange chromatography (Mono S, Amersham Biosciences).

To incorporate selenomethionine into the α-catenin 385–651 fragment, the expression vector was transformed into the methionine aux-otroph strain B834 (Novagen). Cells were grown in defined medium containing 250 μM selenomethionine and supplemented with Kao and Michayluk vitamin solution (Sigma).

Crystallization and Data Collection

Crystals of selenomethionine-labeled α-catenin 385–651 were grown at room temperature in an anaerobic chamber by the hanging drop vapor diffusion method, by mixing 1 μl of a 80 mg/ml protein solution with 1 μl of the well solution containing 700 mM sodium acetate, pH 4.0, 10 mM dithiothreitol, 1.05 M urea, 200 mM sodium/potassium tartrate, and 3% isopropanol. Crystals grew from a heavy precipitate. Crystals were adapted for cryoprotection by transfer into synthetic mother liquor solutions containing 5% step increases of ethylene glycol to a final concentration of 30% and frozen in a 100 K nitrogen gas stream. The crystals belong to the space group $P2_12_12_1$ with unit cell dimension a = 64.8 Å, b = 105.3 Å, and c = 123.9 Å. There are three molecules in the asymmetric unit, corresponding to a solvent content of 48%. Typical dimensions of the crystals were 200 × 200 × 150 μm.

Diffraction data were measured from a single crystal at beamline 1–5 of the Stanford Synchroton Radiation Laboratory. Complete data to 2.5 Å Bragg spacings were collected at four wavelengths at 120 s per 1° exposure on an ADSC Quantum 4 CCD detector. Data were integrated and scaled using Denzo and Scalepack (30). Data collection statistics are presented in Table I.

Structure Determination and Refinement

Patterson and phasing calculations were performed with the program CNS (31); model building was done with the program O (32). An automated Patterson search revealed five sites, and two additional sites were identified from anomalous and dispersive difference Fourier maps calculated with phases made from the five-site model, giving a total of 7 out of 21 possible sites. Solvent flipping did not significantly improve the phases and was therefore not used. The electron density map calculated from the multi-wavelength anomalous dispersion phases was of sufficient quality to assign the sequence for most of the model. To reduce model bias, the initial rounds of refinement were carried out using the complex structure factors (MLHL target in CNS). After seven rounds of refinement the model was refined against the edge data set with a maximum likelihood target using amplitudes only. Bulk solvent and anisotropic temperature factor corrections were applied during all rounds of refinement. After several rounds of minimization and two rounds of simulated annealing, all side chains could be placed. Non-crystallographic symmetry restraints, even at a low weight, resulted in higher *R*-factors and were therefore not used. Individual temperature factors were refined in the later stages of refinement. The limited resolution precluded extensive modeling of water molecules, but a limited number of water molecules could be identified as $F_o - F_c$ peaks above 3 standard deviations with sensible hydrogen bonding geometry. Phasing and refinement statistics are shown in Table I.

Cross-linking Experiments

Purified protein was concentrated and dialyzed against 100 mM HEPES, pH 8.0; dilutions required to adjust the protein concentration were made with the same buffer. In a final reaction volume of 30 μl, protein samples were incubated for 1 h at room temperature with a 30-fold excess of the cross-linker DMS (dimethyl suberimidate) or BS3 (bis(sulfosuccinimidyl)suberate) (Pierce). After incubation, samples were immediately boiled in gel loading buffer and separated on a 12% polyacrylamide gel in the case of α-catenin 385–651 and a 15% polyacrylamide gel in case of the two smaller fragments. Gels were stained with Coomassie Blue.

Afadin Binding Assays

MDCK cells were cultured in Dulbecco's modified Eagle's medium, supplemented with 10% (v/v) heat-inactivated fetal calf serum at 37 °C in 10% CO_2 atmosphere. Approximately 70% confluent MDCK cells were washed twice with ice-cold phosphate-buffered saline, containing 50 μM $CaCl_2$. Cells were scraped from the plate into ice-cold phosphate-buffered saline and pelleted by centrifugation at 2000 × *g* for 5 min at 4 °C. The pellet was resuspended in Nonidet P-40 lysis buffer (50 mM Tris, pH 7.5, 150 mM NaCl, 1 mM EDTA, 1% Nonidet P-40, 1 mM DTT, 0.2 mM phenylmethylsulfonyl fluoride, and 0.2 mM benzamidine), and the cells were lysed for 30 min on ice. The lysate was cleared by centrifugation for 30 min at 1600 × *g* at 4 °C. GST fusion proteins were coupled to glutathione-agarose at a concentration of 4.75×10^{-9} M/200 μl of 50% bead suspension. 80 μl of a 50% bead suspension were incubated for 2 h at 4 °C with lysate obtained from two 15-cm diameter culture plates. Beads were washed four times with 500 μl of Nonidet P-40 lysis buffer and boiled in 40 μl of SDS loading buffer. Samples were run on a 7% polyacrylamide gel and subsequently electroblotted onto a nitrocellulose membrane. After blocking with 20 mM Tris, pH 7.5, 100 mM NaCl, 0.1% Tween 20 containing 5% nonfat

dry milk, the membranes were incubated with a monoclonal mouse anti-l-afadin antibody, followed by incubation with a secondary horseradish peroxidase-coupled anti-mouse antibody. Bands were visualized with the ECL detection system (Amersham Biosciences).

Actin Cosedimentation Assay

Monomeric rabbit skeletal muscle actin (Cytoskeleton Inc., Denver, CO) was stored in 5 mM Tris, pH 8.0, 0.2 mM $CaCl_2$, 0.5 mM DTT, and 0.2 mM ATP at a concentration of 0.4 mg/ml (9.5 μM). 50-μl aliquots were polymerized by addition of 5 μl of 10-fold concentrated actin polymerization buffer (500 mM KCl, 20 mM $MgCl_2$, and 10 mM ATP) and incubation for 1 h at room temperature. Protein stocks used in the following step were precleared by centrifugation at 436,000 × *g* for 7 min to exclude cosedimentation of aggregates. After the addition of 5 μl of protein stock solution (100 μM) to the polymerized actin aliquots, samples were incubated for 30 min at room temperature. Protein bound to F-actin was separated from unbound protein by centrifugation at 436,000 × *g* at 4 °C for 7 min. 30 μl of the supernatant were mixed with 10 μl of 4× gel loading buffer, boiled, and loaded on a 12% polyacrylamide gel. The pellet was resuspended in 60 μl of gel loading buffer, boiled, and 30 μl were loaded onto a gel. Gels were stained with Coomassie Blue.

RESULTS

Structure of α-Catenin 385–651

Limited proteolysis was used to define stable fragments of α-catenin (25). Incubation of full-length α-catenin with trypsin results in the accumulation of two fragments that encompass residues 82–287 and residues 385–651. The α-catenin 82–279 fragment constitutes the dimerization and β-catenin-binding region of α-catenin, whose structure and interactions with β-catenin were described previously (25). The structure of α-catenin 385–651 was solved by multiwavelength anomalous dispersion phasing and refined to 2.5-Å resolution (Table I). There are three copies of the molecule in the asymmetric unit, which are related by a 91° and a 112° rotation. The final model consists of residues 388 – 601 and 606 – 631 for copy A, residues 391–562, 566 –597, and 607–631 for copy B, and residues 393–600 and 607–631 for copy C. Residues 632–651 are never observed, indicating that they are disordered, which is consistent with the presence of a tryptic cleavage site at residue 633 (27).

The structure of α-catenin 385–651 consists of two four-helix bundles that lie at a relative angle of ~40° (Fig. 1*A*). The first helix in the N-terminal four-helix bundle is shorter than the remaining three (11 residues compared with 26 –30 residues). Residues preceding amino acid 396 turn away from the four-helix bundle, and residues 385–390 and 385–392 in copies B and C are not visible, indicating that this region is flexible. In both four-helix bundles, the third helix contains a proline residue, which causes a prominent kink. The proline in the C-terminal four-helix bundle additionally causes the turn preceding the proline to bulge (Fig. 1*A*).

The small interaction interface between the two four-helix bundles (varying between 464 and 697 $Å^2$) appears to allow for flexibility between the two domains. In the three crystallographically independent views of the molecule, the relative orientation of the two subdomains differs by up to 14°. In the recently published structure of the α-catenin M-fragment (27), residues 377–633, the asymmetric unit contains two copies of the molecule; in both, the two domains assume an almost perpendicular orientation and their disposition with respect to each other varies by 10°. Comparison of the two crystal structures shows that the angle between the two bundles varies up to 56° (Fig. 1*B*). The relative orientation of the two domains therefore exhibits a much wider range than expected from the single structures.

The "closed" conformation seen in the present structure is stabilized by side by side interactions between the two four-helix bundles, whereas the "open" conformation seen in the M-fragment is stabilized by interactions between the bases of the four-helix bundles. In both the closed and the open conformations, the number of contacts between the two four-helix bundles is rather small, and the maximum surface area buried between the bundles is 697 and 680 $Å^2$, respectively.

Oligomeric State of α-Catenin 385–651

α-Catenin 385–651 and the α-catenin M-fragment (27) (residues 377–633) were crystallized under different conditions and in two different crystal forms. In each case there are multiple copies of the molecule in the asymmetric unit. The surface area buried between molecules is 866, 1788, and 2317 $Å^2$ between copies A and C, A and B, and B and C, respectively, in the α-catenin 385–651 crystals. In the α-catenin 377–633 crystals, 1280 $Å^2$ of solvent-accessible surface area is buried in the non-crystallographic dimer interface. Although the dimers seen in the M-fragment crystals (27) are formed by two molecules in the open conformation, modeling indicates that the dimer interactions would be possible in the closed conformation. Conversely, the trimers observed in the present crystals are formed by molecules in the closed conformation; molecules in the open conformation could not form the trimer interactions without steric clashes.

To assess the possible relevance of the crystallographically observed oligomers, we examined the properties of the α-catenin 385–651 fragment in solution. Oligomerization of α-catenin 385–651 or 377–633 cannot be detected by gel filtration chromatography (data not shown; see also Ref. 27). However, a small fraction of α-catenin 385–651 can be cross-linked to dimers and trimers at protein concentrations above 100 μM (Fig. 2). Cross-linking to dimers and trimers is also observed with α-catenin 377–633 (27). The contacts seen in the asymmetric unit of the α-catenin 385–651 crystals mostly involve the N-terminal four-helix bundle, whereas those observed in the α-catenin 377–633 crystals solely involve interactions between the C-terminal four-helix bundles (27). We expressed the N- and C-terminal domains separately and confirmed their correct folding by circular dichroism spectroscopy (data not shown). Consistent with the crystal packing, the C-terminal bundle (residues 507–632) can be cross-linked to dimers at protein concentrations above 20 μM, whereas for the N-terminal domain α-catenin 385–507 cross-links to trimers, but not to dimers, at concentrations above 100 μM (Fig. 2).

α-Catenin 385–651 Includes the l-Afadin-binding Site

Yeast two-hybrid and *in vitro* binding assays have shown that the C-terminal half of α-catenin, α-catenin 509–906, interacts directly with l-afadin (21). To more precisely map the l-afadin-binding site on α-catenin, different GST-α-catenin fusion proteins were coupled to glutathione-agarose beads and incubated with MDCK cell lysate. Binding of l-afadin was assessed by Western blotting (Fig. 3*B*). The C-terminal α-catenin fragment used in previous binding studies (21) includes the second four-helix bundle of α-catenin 385–651, so we tested α-catenin 385–651 for l-afadin binding. To assess the contribution of the C terminus of α-catenin we generated two C-terminal fragments (Fig. 3*A*). In the structure of α-catenin 385–651, the last ordered residue is 631, and we therefore prepared a construct comprising residues 632–906. This fragment degraded to a smaller fragment starting at residue 671 during thrombin cleavage of the GST fusion protein, so a second construct encompassing residue 671–906 was also prepared and tested. No binding was detectable for α-catenins 632–906 and 671–906 or the GST control, whereas α-catenin 385–651 clearly bound l-afadin (Fig. 3*B*). In our binding assay 1% of the total amount of l-afadin detected in the cell extract was found to be bound to α-catenin 385–651. To further refine the l-afadin-binding site, GST fusion proteins of the N- and C-terminal four-helix bundle subdomains of the

fragment were prepared and tested in the same binding assay (Fig. 3*C*). The interaction of l-afadin with the N-terminal four-helix bundle was barely detectable, whereas l-afadin bound to the C-terminal four-helix bundle. However, compared with the α-catenin 385–651 fragment, this interaction is significantly weaker. Combined with the observation that the N-terminal half of α-catenin, α-catenin 1–508, does not bind to l-afadin, these data indicate that α-catenin 385–651 constitutes the full binding site for l-afadin. We were also able to detect l-afadin binding to full-length α-catenin (Fig. 3, *B* and *C*). However, significantly less l-afadin bound to the full-length protein compared with the fragment α-catenin 385–651.

The Actin-binding Domain of α-Catenin

The actin-binding site of α-catenin has been mapped by *in vitro* binding assays to residues 461–906 (9) and has been further narrowed down to residues 697–906 by *in vivo* actin colocalization studies (12). α-Catenin is homologous to the F-actin-binding protein vinculin, and the region of strongest homology corresponds to the C-terminal actin-binding domain of vinculin. We tested three C-terminal fragments of α-catenin for F-actin binding: α-catenin 632–906 and α-catenin 671–906 (see above) and α-catenin 678 – 864. The borders of α-catenin 678 – 864 were chosen by homology to the vinculin tail domain (26) (Fig. 4*A*). Proper folding was assessed by circular dichroism spectroscopy for α-catenin 631–906 and 678 – 864 (data not shown). Whereas the two fragments that extend to the very C terminus of α-catenin both bind to F-actin, α-catenin 678 – 864 does not cosediment with actin (Fig. 4*B*). Therefore, it appears that the C-terminal 42 amino acids of α-catenin that extend beyond the vinculin homology region are required for binding to F-actin.

DISCUSSION

The proper organization of adherens junctions in epithelial cells involves the clustering and cytoskeletal anchorage of cadherin molecules and their colocalization with the nectin adhesion system (20). α-Catenin binds to F-actin and to l-afadin and thus has essential roles in these processes. In the studies presented here, the regions of α-catenin responsible for binding to l-afadin and F-actin have been defined biochemically and structurally.

The structure of the proteolytically defined α-catenin fragment, α-catenin 385–651, consists of two adjacent four-helix bundles. Each four-helix bundle has the ability to oligomerize. Packing of molecules in the crystals and cross-linking experiments indicate that at high concentrations the N-terminal bundle can trimerize, whereas the C-terminal bundle can dimerize. These results are consistent with the observation that the entire fragment can be crosslinked to dimers and trimers (27) (Fig. 2). The size of most of the interfaces between the different copies of the protein in the crystallographic asymmetric unit are in a range typical for specific protein-protein interactions (33). However, the contacts are unique to each crystal form. Furthermore, oligomerization cannot be detected by gel filtration chromatography, which indicates a low affinity interaction. Therefore, the biological significance of this self-association remains unclear. Amino acids 509 – 643, which comprise the C-terminal four-helix bundle, have been shown to play a significant role in modulating cell adhesion (14). This function might be related to the ability of the C-terminal domain to dimerize, which might ultimately cause a clustering of cadherin cell adhesion molecules (27).

The relative orientation of the two four-helix bundles of the α-catenin 385–651 fragment exhibits a surprising variability, which is likely due to the small number of contacts between these two subdomains. Within one crystal form, the inter-bundle angles vary modestly, up to 14°. More strikingly, comparison of the structure in the present crystal form to that of the M-fragment (27) shows that the angular arrangement changes from a relative rotation of about 40° (the closed conformation) to an approximately perpendicular arrangement of the two

bundles (the open conformation) (Fig. 1*B*). Each of these conformations is stabilized by a different set of interdomain contacts, and conformations in which neither set of contacts are present are likely to be energetically less favorable. It is tempting to speculate that a switch between these two conformations mediates a regulatory function, although it is possible that steric hindrance by other domains in the full-length molecule restricts this large interdomain movement.

We have shown that α-catenin 385–561 includes the full binding site for l-afadin. The observation that the isolated four-helix bundles bind no or less l-afadin than the entire fragment indicates that both four-helix bundles contribute to the l-afadin-binding site. Full-length α-catenin bound significantly less l-afadin than the α-catenin fragment 385–651. In a previous study, only the C-terminal half of α-catenin (residues 508–906), but not the full-length protein, bound to l-afadin (21). Those experiments, which included yeast two-hybrid analysis and *in vitro* binding assays with recombinant proteins and subsequent protein detection by Coomassie staining, might not have been sensitive enough to detect the binding of full-length protein (21). Collectively, these data indicate that there is a cryptic binding site for l-afadin in full-length α-catenin.

The structural and biochemical data presented here suggest two possible mechanisms for regulating l-afadin binding. In one scenario, the open and closed conformations observed in the crystals of α-catenin 385–651 and α-catenin 377–633 (27) represent active and inactive states for l-afadin binding. In this case, the switch between these conformations would affect the l-afadin binding surface formed by the two four-helix bundles. In the full-length protein, other domains could impose steric constraints on the switch between open and closed conformation and thereby cause a reduction in l-afadin binding, whereas the two conformations might be more easily interchangeable in the fragment. Alternatively, the arrangement of other domains in the full-length protein might not allow the large interdomain movement observed in the crystals, so that the l-afadin-binding region possesses only one conformation. In this case, the observation that the l-afadin-binding site is flexibly linked to the flanking regions of α-catenin, as indicated by proteolytic sensitivity (25), suggests that interdomain movements regulate access to the l-afadin-binding site.

Conformational changes leading to the exposure of the l-afadin-binding site in the full-length protein could in principle be regulated by a variety of possible mechanisms, such as phosphorylation/dephosphorylation or the interaction with other α-catenin-binding proteins. In addition, self-association, either through the N-terminal α-catenin dimerization domain (25) or through the l-afadin-binding domain described above, could affect accessibility of the l-afadin-binding site. For example, α-catenin forms a dimer in solution which dissociates upon binding to β-catenin (25, 34), and α-actinin binds to α-catenin only when α-catenin is associated with β-catenin (35). This observations might indicate the presence of a cryptic binding site for α-actinin that is masked in the α-catenin dimer and activated through β-catenin binding.

Cryptic binding sites have been identified in several other proteins that are involved in tethering of transmembrane proteins to the actin cytoskeleton. Interactions between the head and tail domain of vinculin mask binding sites on both domains (36). The C-terminal actin-binding domain of vinculin forms a five-helix bundle, which appears to open to a less tightly packed conformation when bound to F-actin (26). It has been suggested that the interaction between head and tail domain prevents this conformational change and thereby allosterically controls association of vinculin with F-actin (26). Similarly, in proteins of the ERM (ezrin/radixin/moesin) family, interaction between the FERM head domain and the tail domain masks the binding sites for other proteins (37), and conformational activation involves a weakening of the head-to-tail interaction. In ERM proteins the association of head and tail

domain determines the conformation of the tail domain, and it has been suggested that the tail domain adopts a different conformation when it binds to actin (38).

Vinculin shares sequence and most likely structural similarity with α-catenin, including the portion of the α-catenin dimerization and the afadin-binding domain (25, 27). The two proteins share the highest degree of sequence identity within the actin-binding domain of vinculin (27%), which is a five-helix bundle (26, 27). However, α-catenin contains an additional 42 amino acids C-terminal to the bundle homology region. Deletion of these amino acids impairs actin binding (Fig. 4*B*) but does not affect folding of α-catenin 678–864. This result indicates that the C-terminal 42 amino acids are involved directly in actin binding. In contrast to vinculin, the actin-binding site in α-catenin is not masked, and binding affinities for the α-catenin-actin interaction are about 10-fold higher for the full-length protein (about 0.3 μM) compared with a fragment that includes the C-terminal 447 amino acids (about 3 μM) (9). Taken together, these data indicate that even though α-catenin and vinculin share sequence and probably structural similarity, the two proteins differ in their interaction with F-actin.

Acknowledgments

We thank S. Fridman for technical assistance and H. Bellamy for beamline support.

References

1. Gumbiner BM. Cell. 1996; 84:345–357. [PubMed: 8608588]
2. Tomschy A, Fauser C, Landwehr R, Engel J. EMBO J. 1996; 15:3507–3514. [PubMed: 8670853]
3. Brieher WM, Yap AS, Gumbiner BM. J Cell Biol. 1996; 135:487–496. [PubMed: 8896604]
4. Steinberg MS, McNutt PM. Curr Opin Cell Biol. 1999; 11:554–560. [PubMed: 10508659]
5. Adams CL, Nelson WJ, Smith SJ. J Cell Biol. 1996; 135:1899–1911. [PubMed: 8991100]
6. Angres B, Barth A, Nelson WJ. J Cell Biol. 1996; 134:549–557. [PubMed: 8707837]
7. Ozawa M, Kemler R. J Cell Biol. 1992; 116:989–996. [PubMed: 1734027]
8. Jou TS, Stewart DB, Stappert J, Nelson WJ, Marrs JA. Proc Natl Acad Sci U S A. 1995; 92:5067–5071. [PubMed: 7761449]
9. Rimm DL, Koslov ER, Kebriaei P, Cianci CD, Morrow JS. Proc Natl Acad Sci U S A. 1995; 92:8813–8817. [PubMed: 7568023]
10. Itoh M, Nagafuchi A, Moroi S, Tsukita S. J Cell Biol. 1997; 138:181–192. [PubMed: 9214391]
11. Itoh M, Morita K, Tsukita S. J Biol Chem. 1999; 274:5981–5986. [PubMed: 10026224]
12. Weiss EE, Kroemker M, Rudiger AH, Jockusch BM, Rudiger M. J Cell Biol. 1998; 141:755–764. [PubMed: 9566974]
13. Watabe-Uchida M, Uchida N, Imamura Y, Nagafuchi A, Fujimoto K, Uemura T, Vermeulen S, van Roy F, Adamson ED, Takeichi M. J Cell Biol. 1998; 142:847–857. [PubMed: 9700171]
14. Imamura Y, Itoh M, Maeno Y, Tsukita S, Nagafuchi A. J Cell Biol. 1999; 144:1311–1322. [PubMed: 10087272]
15. Pradham D, Lombardo CR, Roe S, Rimm DL, Morrow JS. J Biol Chem. 2001; 276:4175–4181. [PubMed: 11069925]
16. Takahashi K, Nakanishi H, Miyahara M, Mandai K, Satoh K, Satoh A, Nishioka H, Aoki N, Mizoguchi A, Takai Y. J Cell Biol. 1999; 145:539–549. [PubMed: 10225955]
17. Mandai K, Nakanishi H, Satoh A, Takahashi K, Satoh K, Nishioka H, Mizoguchi A, Takai Y. J Cell Biol. 1999; 144:1001–1017. [PubMed: 10085297]
18. Mandai K, Nakanishi H, Satoh A, Obaishi H, Wada M, Nishioka M, Itoh M, Mizoguchi A, Aoki T, Fujimoto T, Matsuda Y, Tsukita S, Takai Y. J Cell Biol. 1997; 139:517–528. [PubMed: 9334353]
19. Miyahara M, Nakanishi H, Takahashi K, Satoh-Horikawa K, Tachibana K, Takai Y. J Biol Chem. 2000; 275:613–618. [PubMed: 10617658]

20. Ikeda W, Nakanishi H, Miyoshi J, Mandai K, Ishizaki H, Tanaka M, Togawa A, Takahashi K, Nishioka H, Yoshida H, Mizoguchi A, Nishikawa S, Takai Y. J Cell Biol. 1999; 146:1117–1131. [PubMed: 10477764]
21. Tachibana K, Nakanishi H, Mandai K, Ozaki K, Ikeda W, Yamamoto Y, Nagafuchi A, Tsukita S, Takai Y. J Cell Biol. 2000; 150:1161–1175. [PubMed: 10974003]
22. Sakisaka T, Nakanishi H, Takahashi K, Mandai K, Miyahara M, Satoh A, Takaishi K, Takai Y. Oncogene. 1998; 18:1609–1617. [PubMed: 10102631]
23. Nagafuchi A, Takeichi M, Tsukita S. Cell. 1991; 65:849–857. [PubMed: 1904011]
24. Herrenknecht K, Ozawa M, Eckerskorn C, Lottspeich F, Lenter M, Kemler R. Proc Natl Acad Sci U S A. 1991; 88:9156–9160. [PubMed: 1924379]
25. Pokutta S, Weis WI. Mol Cell. 2000; 5:533–543. [PubMed: 10882138]
26. Bakolitska C, de Pereda JM, Bagshaw CR, Critchley DR, Liddington RC. Cell. 1999; 99:603–613. [PubMed: 10612396]
27. Yang J, Dokurno P, Tonks NK, Barford D. EMBO J. 2001; 20:3645–3656. [PubMed: 11447106]
28. Aberle H, Butz S, Stappert J, Weissig H, Kemler R, Hoschuetzky H. J Cell Sci. 1994; 107:3655–3663. [PubMed: 7706414]
29. Guan KL, Dixon JE. Biochemistry. 1991; 192:262–267.
30. Otwinowski Z, Minor W. Methods Enzymol. 1997; 276:307–326.
31. Brünger AT, Adams PD, Clore GM, Gros P, Grosse-Kunstleve RW, Jiang JS, Kuszewsky J, Nilges M, Pannu NS, Read RJ, Rice LM, Simoson T, Warren GL. Acta Crystallogr Sect D Biol Crystallogr. 1998; 54:905–921. [PubMed: 9757107]
32. Jones TA, Zou JY, Cowan SW, Kjeldgaard M. Acta Crystallogr Sect A. 1991; 47:110–119. [PubMed: 2025413]
33. Lo Conte L, Chothia C, Janin J. J Mol Biol. 1999; 285:2177–2198. [PubMed: 9925793]
34. Koslov ER, Maupin P, Pradhan D, Morrow JS, Rimm DL. J Biol Chem. 1997; 272:27301–27306. [PubMed: 9341178]
35. Knudsen KA, Soler AP, Johnson KR, Wheelock MJ. J Cell Biol. 1995; 130:67–77. [PubMed: 7790378]
36. Craig SW, Johnson RP. Nature. 1995; 373:261–264. [PubMed: 7816144]
37. Tsukita S, Yonemura S, Tsukita S. Trends Biol Sci. 1997; 22:53–58.
38. Pearson MA, Reczek D, Bretscher A, Karplus PA. Cell. 2000; 101:259–270. [PubMed: 10847681]
39. Kraulis PJ. J Appl Crystallogr. 1991; 24:946–950.
40. Merritt EA, Murphy MEP. Acta Crystallogr Sect D Biol Crystallogr. 1994; 50:869–873. [PubMed: 15299354]

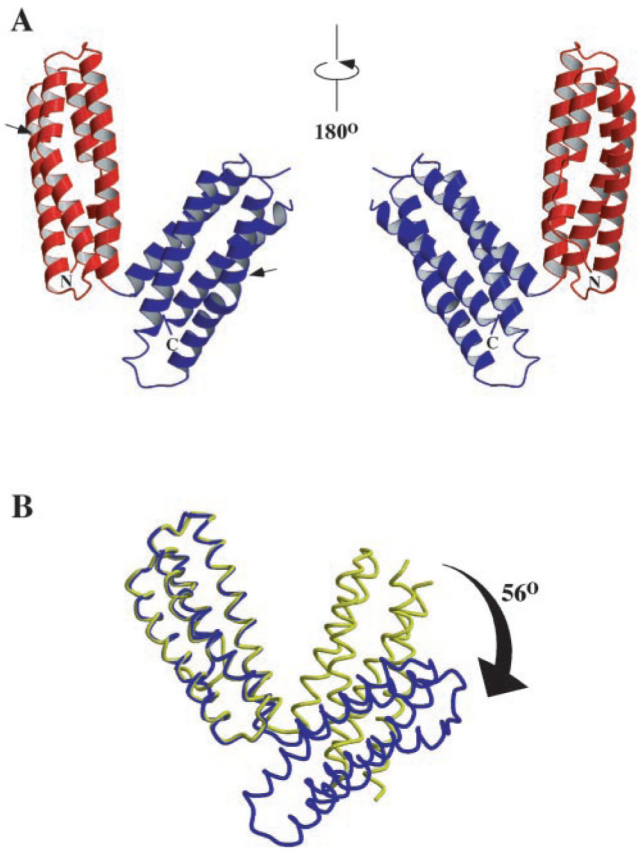

Fig. 1. Structure of α-catenin 385–651

A, ribbon diagram of the structure; the two views of the molecule rotated by 180°. The N- and C-terminal four-helix bundles are colored in *red* and *blue*, respectively. These subdomains correspond to the N- and C-terminal fragments used in cross-linking and afadin binding studies. The positions of proline residues within the helices are indicated by an *arrow*. *B*, relative motion of the N- and C-terminal subdomains of α-catenin 385–651. The N-terminal subdomains of the α-catenin 385–651 fragment (*yellow*) and the α-catenin M fragment (Ref. 27; residues 377–633) (*blue*) were superimposed. The relative orientation of the N- and C-terminal domain varies in the five different views obtained from the two different crystal forms. The two copies shown here show the largest angular displacement between the two four-helix bundles. The figure was prepared using MOLSCRIPT (39) and RASTER3D (40).

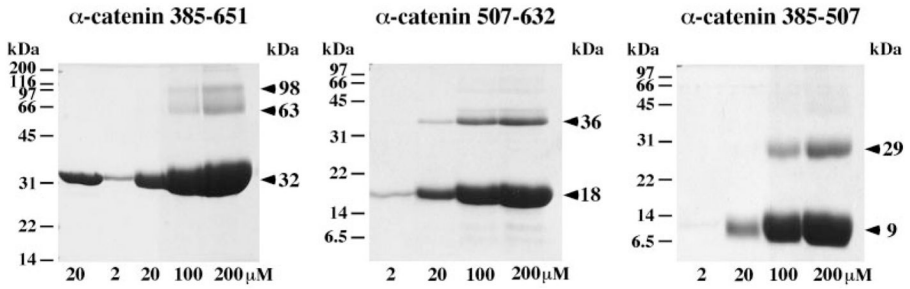

Fig. 2. Oligomerization of *α*-catenin 385–651 and its N- and C-terminal subdomains

Fragments at the indicated concentrations were incubated with a 30-fold excess of cross-linker. For the two amine-reactive cross-linking reagents BS3 and DMS with spacer arms of 11.4 and 11.0 Å, respectively, different cross-linking efficiency was observed. Higher cross-linking efficiency results are shown here and were obtained with DMS in the case of *α*-catenin 507–632 and BS3 for *α*-catenin 385–651 and *α*-catenin 385–507. The *first lane* for the *α*-catenin 385–651 fragment shows a sample in the absence of cross-linker. Molecular mass markers are indicated on the *left* of each gel, and apparent molecular mass of the fragments and cross-linking products are shown on the *right*.

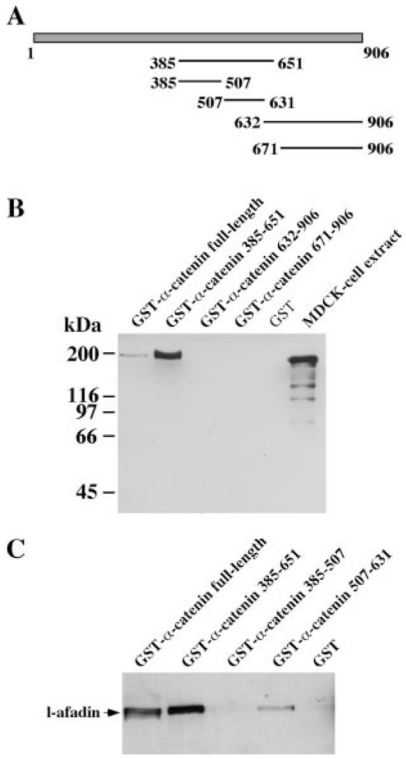

Fig. 3. Interaction of α-catenin with l-afadin

A, schematic representation of the different α-catenin fragments used in the binding assays. *B*, proteins expressed as GST fusion proteins were coupled to glutathione-agarose beads and incubated with MDCK cell lysate. Bound protein was analyzed by Western blotting using monoclonal anti-afadin antibody. The signal for l-afadin in 15 μl of MDCK lysate, which corresponds to 1% of the amount used in the binding assays, is shown in the *right lane*. Molecular mass markers are shown on the *left*. *C*, binding to the N- and C-terminal subdomains of α-catenin 385–651.

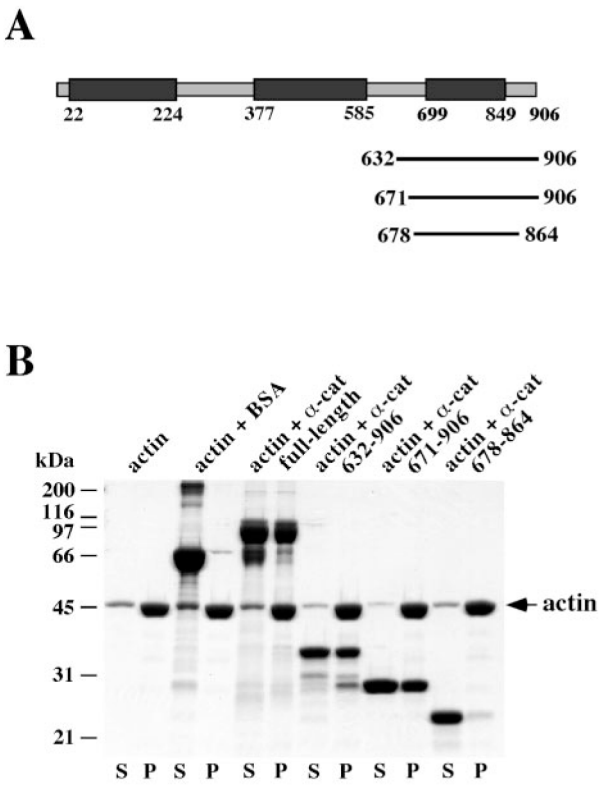

Fig. 4. Interaction of α-catenin (*α-cat*) with F-actin

A, schematic representation of α-catenin and the constructs used in the binding assay. Vinculin homology regions are shown in *dark gray*. *B*, binding to F-actin was examined by cosedimentation. Assuming a binding ratio of protein:monomeric actin of 1:7, all α-catenin constructs were added in excess. The supernatant (*S*) containing the unbound protein and the pellet (*P*) containing F-actin and bound protein are shown for each sample. Molecular mass markers are indicated on the *left*.

Table I

Crystallographic data α-catenin 385–651

r.m.s.d., root mean square deviation.

A. Data collection[a]

Wavelength (Å)	Resolution	% complete	R_{sym}[b]	% > 3σ/(I)	Average redundancy
λ1 = 0.9252 (remote)	30.0–2.5	99.6 (99.2)	0.039 (0.254)	84.9 (57.6)	3.9 (3.9)
λ2 = 0.9795 (peak)	30.0–2.5	99.8 (100)	0.037 (0.248)	86.5 (61.0)	4.4 (4.3)
λ3 = 0.9799 (edge)	30.0–2.5	99.9 (100)	0.035 (0.237)	87.0 (62.5)	4.3 (4.3)
λ4 = 1.0688 (remote)	30.0–2.5	99.8 (99.9)	0.036 (0.265)	85.8 (58.5)	4.3 (4.2)

B. Phasing statistics

Wavelength	Anomalous diffraction ratios[c]				Phasing power[d]	
	λ1	λ2	λ3	λ4	+ Friedel mate	− Friedel mate
λ1	0.046	0.045	0.051	0.047	0.52	0.88
λ2		0.052	0.041	0.049	1.12	1.50
λ3			0.039	0.040	1.30	1.52
λ4				0.040	reference	0.45

Resolution (Å)	29.95–4.98	4.98–3.95	3.95–3.46	3.46–3.14	3.14–2.92	2.92–2.74	2.74–2.61	2.61–2.49	Overall
Figure-of-merit	0.79	0.75	0.72	0.67	0.61	0.53	0.47	0.40	0.63

C. Refinement statistics

***R* values and temperature factors**		**Model geometry**	
No. reflections:			
Working set[e]	49,464	Bond length r.m.s.d. from ideal	0.007Å
Test set[e]	5428	Bond angle r.m.s.d. from ideal	1.1°
R_{cryst}[f]	0.238	Ramachandran plot:	
R_{free}[f]	0.273	% in most favored regions	92.1%
		% in additional allowed regions	7.9%
No. atoms			
Protein	5457		

C. Refinement statistics

***R* values and temperature factors**		**Model geometry**	
Solvent	90		
Average B (Å^2)			
Protein (copy A/B/C)	49.2/69.6/69.9		
Solvent	40.6		
		Temperature factor r.m.s.d. (Å^2)	
Overall anisotropic B (Å)		Main chain bond-related	1.3
B_{11}	5.0	Main chain angle-related	2.3
B_{12}	−5.1	Main chain bond-related	2.2
B_{33}	0.0	Side chain angle-related	3.3

[a] Values in parentheses are for the highest resolution shell: 2.54–2.50 Å.

[b] $R_{sym} = \Sigma_h\Sigma_i(I_i(h) - \langle I(h)\rangle)|/\Sigma_h\Sigma_i I_i(h)$, where $I_i(h)$ is the ith measurement of reflection h, and $\langle I(h)\rangle$ is the weighted mean of all measurements of h. Bijvoet measurements were treated as independent reflections for the MAD phasing data sets.

[c] Anomalous diffraction ratios = $\langle\Delta|F|\rangle/\langle|F|\rangle$, where $\langle\Delta|F|\rangle$ is the r.m.s. Bijvoet difference at a single wavelength (diagonal elements) or the r.m.s. dispersive difference between two wavelengths (off diagonal elements).

[d] Phasing Power = $\langle|F_H|\rangle/E$, where $\langle|F_H|\rangle$ is the r.m.s. structure factor amplitude for anomalous scatterers, and E is the estimated lack of closure. Phasing power is listed for each lack-of-closure expression between the reference data set (+Friedel mate at $\lambda 3$) and the + or − Friedel set at each wavelength. Phasing powers were calculated using all data between 30.0 and 2.5 Å.

[e] The test set comprises a randomly selected subset of the data (10%) that was not included in the refinement of the model. The working set contains the remaining reflections from the data set.

[f] $R = \Sigma_h||F_{obs}(h)| - |F_{calc}(h)||/\Sigma_h|F_{obs}(h)|$. R_{cryst} and R_{free} were calculated using the working and test reflection sets, respectively.